frontiers | Frontiers in Materials

TYPE Original Research
PUBLISHED 21 March 2025
DOI 10.3389/fmats.2025.1504965

OPEN ACCESS

EDITED BY
Rafael Ramirez-Bon,
National Polytechnic Institute of Mexico (CINVESTAV), Mexico

REVIEWED BY
Chaudhry A. Usman,
Hamad bin Khalifa University, Qatar
Dipayan Pal,
University of California, San Diego, United States

*CORRESPONDENCE
Zareen Akhter,
zareenakhter@yahoo.com
Muhammad Faizan Nazar,
faizan.nazar@ue.edu.pk

RECEIVED 01 October 2024
ACCEPTED 24 February 2025
PUBLISHED 21 March 2025

CITATION
Ashraf AR, Akhter Z, Farid MA, Simon LC, Mahmood K and Nazar MF (2025) Thermal performance customization of polyimide films by nanocomposite engineering with Al_2O_3 and ZnO nanoparticles.
Front. Mater. 12:1504965.
doi: 10.3389/fmats.2025.1504965

Thermal performance customization of polyimide films by nanocomposite engineering with Al_2O_3 and ZnO nanoparticles

Ahmad Raza Ashraf[1], Zareen Akhter[2]*, Muhammad Asim Farid[1], Leonardo C. Simon[3], Khalid Mahmood[2] and Muhammad Faizan Nazar[1]*

[1]Department of Chemistry, Division of Science & Technology, University of Education, Lahore, Pakistan, [2]Department of Chemistry, Quaid-i-Azam University, Islamabad, Pakistan, [3]Department of Chemical Engineering, University of Waterloo, Waterloo, ON, Canada

The fascinating properties of polyimide films, such as outstanding thermal stability, chemical/radiation resistance, excellent mechanical strength, and a low dielectric constant, can be further optimized by inorganic fillers, making them potential candidates for replacing metals/ceramics in modern technologies. In this study, the effect of Al_2O_3 and ZnO nanoparticles (NPs) on the thermal performance of polyimide was evaluated by varying nanoparticle loadings (3%, 5%, 7%, and 9%). The incorporation of nanoparticles within the polyimide matrix was confirmed by wide-angle X-ray diffraction (WAXRD) analysis. Their homogenous distribution throughout the matrix was verified by scanning electron microscopy (SEM) and transmission electron microscopy (TEM). Thermal decomposition of the polyimide matrix started at approximately 400°C, with relatively small weight loss up to 500°C, suggesting significantly high thermal stability. This stability was further improved by the addition of Al_2O_3 nanoparticles, while ZnO nanoparticles lowered the temperature resistance. The isothermal thermogravimetric analysis (TGA) further complemented the results of dynamic TGA as substantially high thermal endurance at 400°C was observed for polyimide nanocomposites, suggesting their capability to withstand elevated temperatures for extended periods. The glass transition temperature of the polyimide matrix was enhanced by both types of nanoparticles in a concentration-dependent manner. The thermal performance of polyimide was significantly affected by nanoparticle concentration.

KEYWORDS

nanocomposite engineering, metal oxide nanoparticles, thermal stability, thermal endurance, glass transition temperature

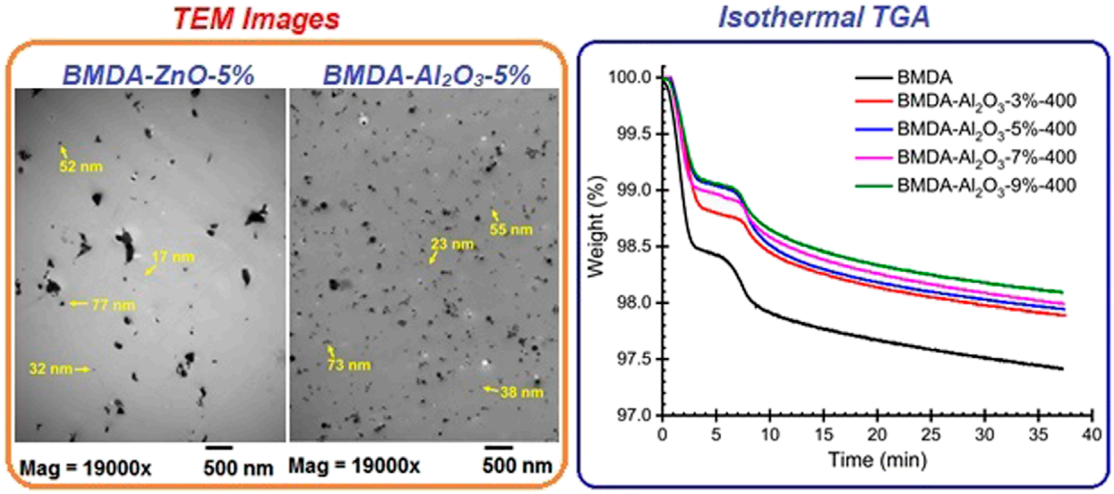

GRAPHICAL ABSTRACT

1 Introduction

Smart manufacturing involves increasing the quality and sustainability of manufacturing activities while reducing costs. This objective is primarily achieved by replacing metals and ceramics with polymers/plastics. However, not every polymer can be used in harsh conditions. Polyimide-based materials have the potential to serve the purpose owing to versatile properties: exceptional thermal stability, impressive stiffness at elevated temperatures, excellent mechanical strength, good radiation and chemical resistance, high glass transition temperature, a low refractive index, and a dielectric constant (Faghihi and Hajibeygi, 2013; Ashraf et al., 2015; Ashraf et al., 2018a; Ashraf et al., 2018b; Mehmood et al., 2024). Furthermore, the incorporation of inorganic nanoparticles (NPs) in a polyimide matrix can tailor its properties as per the need of a particular application (Pavlenko et al., 2019; Kango et al., 2013; Kickelbick, 2003; Kim et al., 2014).

Nanocomposite engineering: the addition of nanofillers into polyimide matrices has greatly influenced the properties of conventional polymers (Ponnamma et al., 2019; Zhang et al., 2022; Ma et al., 2023; Yuan et al., 2024). Nanofillers act as smart dopants for polymers due to their large surface area, modifying the polymer structure by forming a network of organic–inorganic hybrid materials, resulting in fascinating improvements in properties (Lal et al., 2012; Morgan and Putthanarat, 2011; Kim et al., 2013; Zhu et al., 2024). Moreover, the synergistic effect of nanoparticles and the polymer matrix can endow the nanocomposite with significantly improved properties (Nikolaeva et al., 2020). However, there are several challenges associated with dispersing nanoparticles in polymer matrices, e.g., agglomeration of nanoparticles reduces their effectiveness, and low compatibility between nanoparticles and polymer may lead to poor interfacial bonding. Similarly, uniform dispersion becomes more difficult at higher loadings of nanoparticles; hence, properties may deteriorate instead of improving. These challenges can be addressed by the combination of suitable processing techniques (sonication, optimizing processing conditions), appropriate nanoparticle selection, and optimal nanoparticle concentration (Kango et al., 2013; Ponnamma et al., 2019). Therefore, the reinforcement of nanofillers in different polymers is a subject of current interest, aiming to combine the advantageous properties of ceramics and metals into polymeric materials (Wang et al., 2024).

The properties of polyimide nanocomposites rely on the degree of chemical/physical interactions between the host matrix and nanoparticles. The functional groups such as OH on nanoparticles can form Van der Waals forces/electrostatic interactions/hydrogen bonds with the polyimide matrix and can improve the interfacial adhesion between the nanoparticles and polymer (Kango et al., 2013). These interactions can affect the charge transfer complex formation between polyimide chains, thereby altering the matrix properties (Hager et al., 2023; Mathews et al., 2007; Huo et al., 2022). Mallakpour et al. (2014) attributed the red/blue shift in UV spectra to inter-chain hydrogen bonding between hydroxyl (OH) groups on the surface of ZnO nanoparticles with the carbonyl (C=O) of the amide group. Hsu et al. (2005) illustrated the hydrogen bonding interactions between carbonyl (C=O) moieties of imide ring and OH groups on the surface of nanoparticles and observed shift of imide group FTIR frequencies toward lower wavenumbers.

Various types of inorganic nanofillers are being extensively used in developing polyimide/inorganic nanocomposites, e.g., metals (Fe, Al, Ag, and Au), metal oxides (ZnO, TiO_2, NiO, CeO_2, and Al_2O_3), non-metal oxides (SiO_2), and others (SiC and Si_3N_4) (Ma et al., 2023; Nikolaeva et al., 2023; Nikolaeva et al., 2022; Wu et al., 2022; Jeon and Baek, 2010; Chang et al., 2022; Aframehr et al., 2020; Chen et al., 2022; Chen et al., 2020; Gao et al., 2025). The selection of the appropriate nanofiller depends on the desired thermal, mechanical, optical, dielectric, electrical, and/or gas separation properties of the resulting nanocomposites. Ziwei Li et al. developed composite films with improved breakdown field strength and dielectric constant by introducing MgO nanoparticles into the polyimide matrix (Li et al., 2022). The addition of SiO_2 in the polyimide matrix triggered a 10-fold improvement in CO_2 permeability (Rafiq et al., 2012). Polyimide/Fe composite films displayed higher conductivity than those without iron while compromising some of their thermal

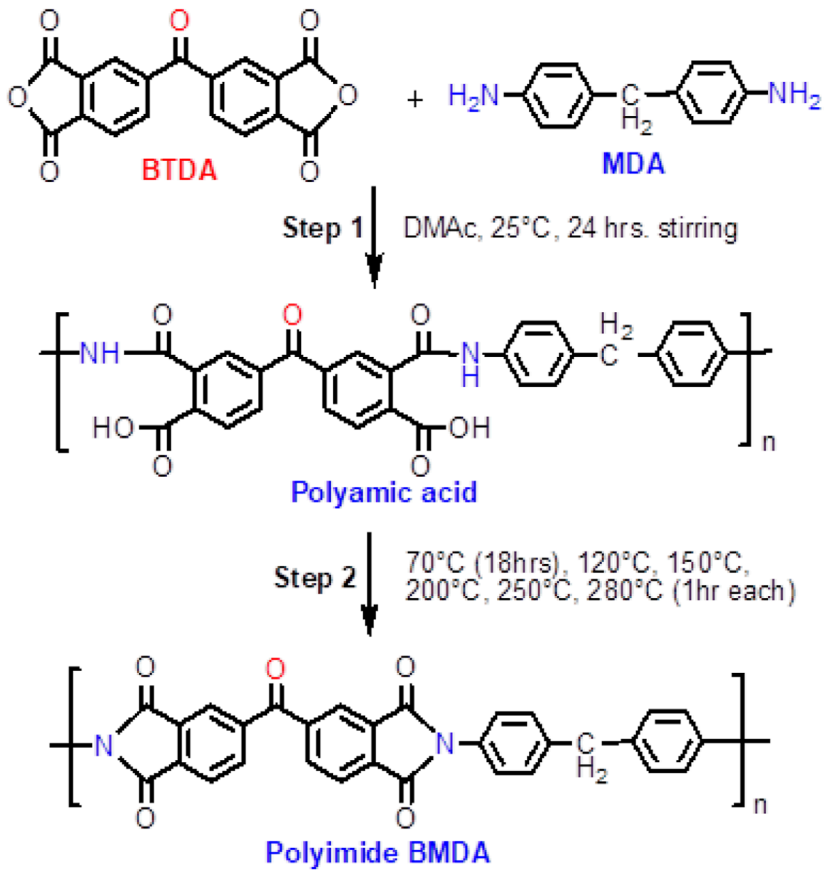

SCHEME 1
Synthesis of the polyimide matrix BMDA.

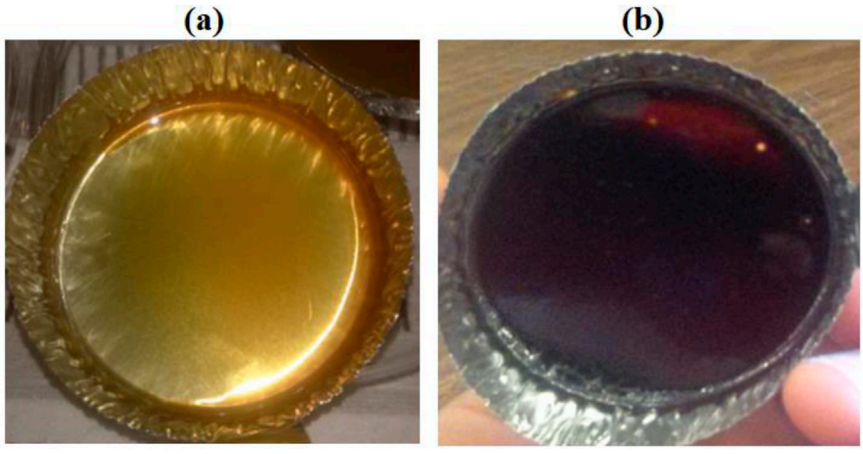

FIGURE 1
Images of films: **(A)** after 70°C treatment and **(B)** at complete imidization.

stability (Elbakoush et al., 2021). Jeon et al. (2018) developed polyimide nanocomposites with a much lower coefficient of thermal extension (CTE) by adding ZnS particles in polyimide films. Enhanced thermal conductivity of polyimide was achieved by the incorporation of TiO_2 in the parent polyimide matrix. Similarly, polyimide hybrids of TiO_2 demonstrated higher glass transition temperature (T_g) and CTE (Lu et al., 2013). Rafiee and Golriz (2015) fabricated polyimide nanocomposites by embedding nanoparticles of α-Fe_2O_3 and observed that nanocomposites displayed better thermal stability compared to parent polyimide (Rafiee and

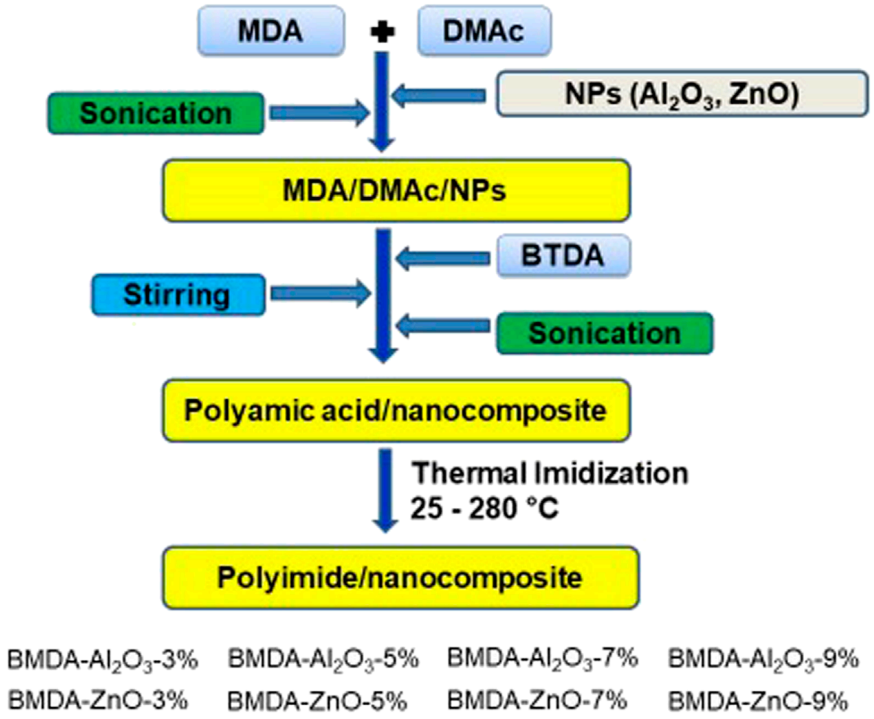

SCHEME 2
Synthesis of polyimide nanocomposites.

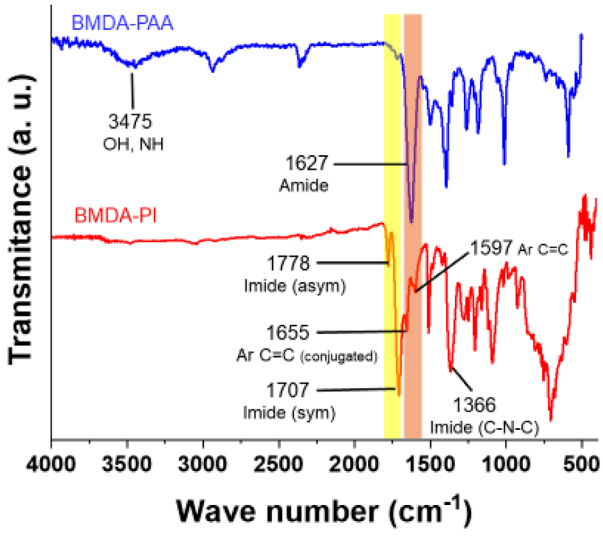

FIGURE 2
FTIR spectrum of BMDA at the polyamic acid stage (BMDA-PAA) and after imidization (BMDA-PI).

Golriz, 2015). The incorporation of TiO_2 nanoparticles within the polyimide matrix modified the polarization phenomenon and improved the charge stability of parent polyimides (Lal et al., 2012).

Among different inorganic nanofillers, Al_2O_3 and ZnO nanoparticles have been selected for the current study due to their several beneficial properties like excellent hardness, UV shielding, high thermal conductance, semiconductor characteristics, and electrical insulation properties (Wang et al., 2022; Mathur et al., 2019; Singh et al., 2019; Singh et al., 2017). Polyimides are known for their high thermal stability, but their thermal conductivity is relatively low compared to other materials like metals/ceramics. The development of polyimide/Al_2O_3 nanocomposites is motivated by the fact that Al_2O_3 nanoparticles have high thermal conductivity, which can enhance the overall thermal conductivity and, ultimately, the thermal stability of the resulting composites (Wang et al., 2022; Ouyang et al., 2022). This improvement is particularly valuable in applications where efficient heat dissipation is crucial, such as in aerospace, electronics, and automotive industries. The ZnO nanoparticles exhibit strong UV absorption properties and are often used in sunscreen products. When incorporated into polyimide, ZnO can provide enhanced UV shielding, which will be beneficial in applications exposed to high-intensity UV radiations, such as space exploration, automotive parts, and solar energy applications, where materials must endure UV radiation while maintaining excellent mechanical and thermal performance (Yousefi et al., 2023; Phatak et al., 2024).

In our previous studies, we tailored the properties of polyimides using different diamines and dianhydride monomers with an emphasis on the structure–property relationship (Ashraf et al., 2015; Ashraf et al., 2018a; Ashraf et al., 2018b). In continuation of our efforts to customize the properties, this article explores the concept of nanocomposite engineering, i.e., the addition of inorganic nanoparticles within a polyimide matrix and monitoring of their effect on the properties of the parent polymer.

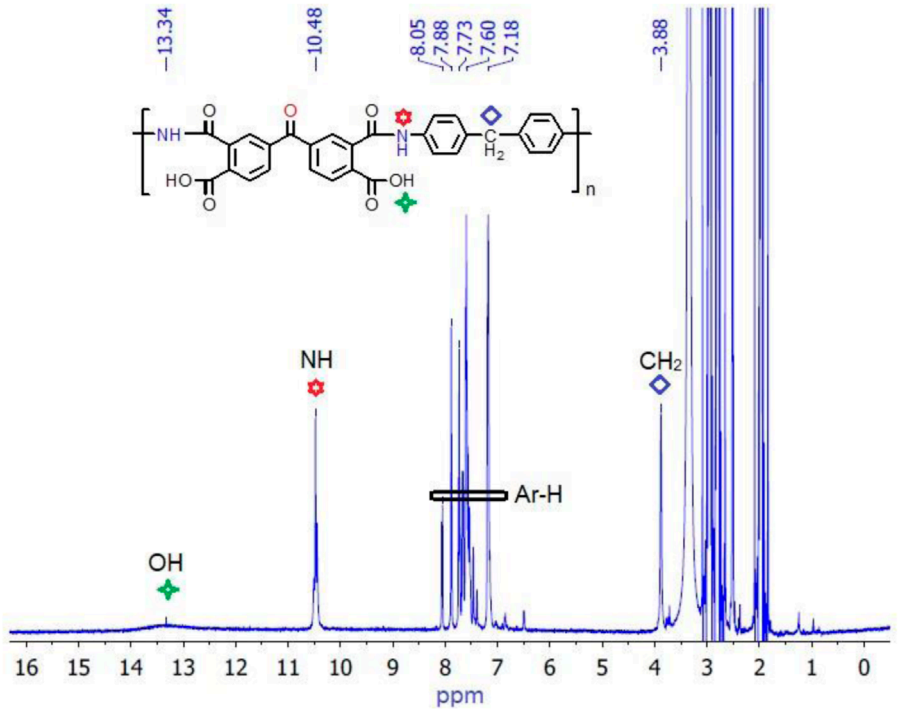

FIGURE 3
Proton NMR spectrum of BMDA at the polyamic acid stage.

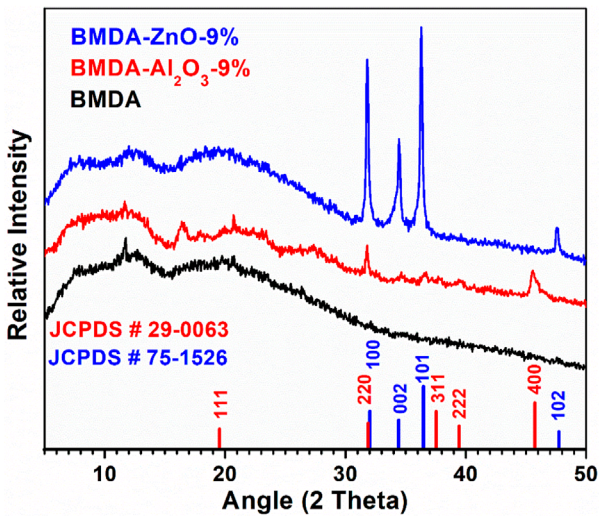

FIGURE 4
WAXRD plots illustrating nanoparticle insertion in polyimide.

The aim of this study was to synthesize metal oxide (Al_2O_3 and ZnO)-based polyimide nanocomposites and monitor the effect of nanoparticle incorporation on temperature resistance, thermal endurance, and glass transition temperature of the polyimide matrix. The structural elucidation of developed composites was carried out by FTIR and NMR spectroscopic techniques, whereas their morphology was studied by wide-angle X-ray diffraction (WAXRD), SEM and TEM analysis. The impact of Al_2O_3 and ZnO nanoparticle incorporation on thermo-oxidative properties of the parent polyimide matrix was investigated by dynamic thermogravimetric analysis (TGA), isothermal TGA, and DMTA under the atmosphere of N_2 and air.

The significance of the study lies in investigating the thermal endurance of the developed nanocomposites for applications involving extended exposure at elevated temperatures; since a heat flux of few minutes would not cause severe degradation of a polymeric system in most cases, However, it may fail, under prolonged exposure to high temperatures. Furthermore, a synthetic protocol was developed to produce nanocomposites with a uniform distribution of nanoparticles throughout the polyimide matrix, eliminating the need for surface modification of nanoparticles for composite synthesis.

2 Experimental setup

2.1 Materials

VWR Canada provided the dianhydride monomer 3,3′,4,4′-benzophenonetetracarboxylic dianhydride, abbreviated as BTDA. The anhydrous solvent N,N-dimethylacetamide (DMAc) and diamine 4,4′-methylenedianiline (MDA) were procured from Sigma-Aldrich, Germany. The nanoparticles of ZnO and Al_2O_3 were acquired from Alfa Aesar and Nanophase Technologies, respectively.

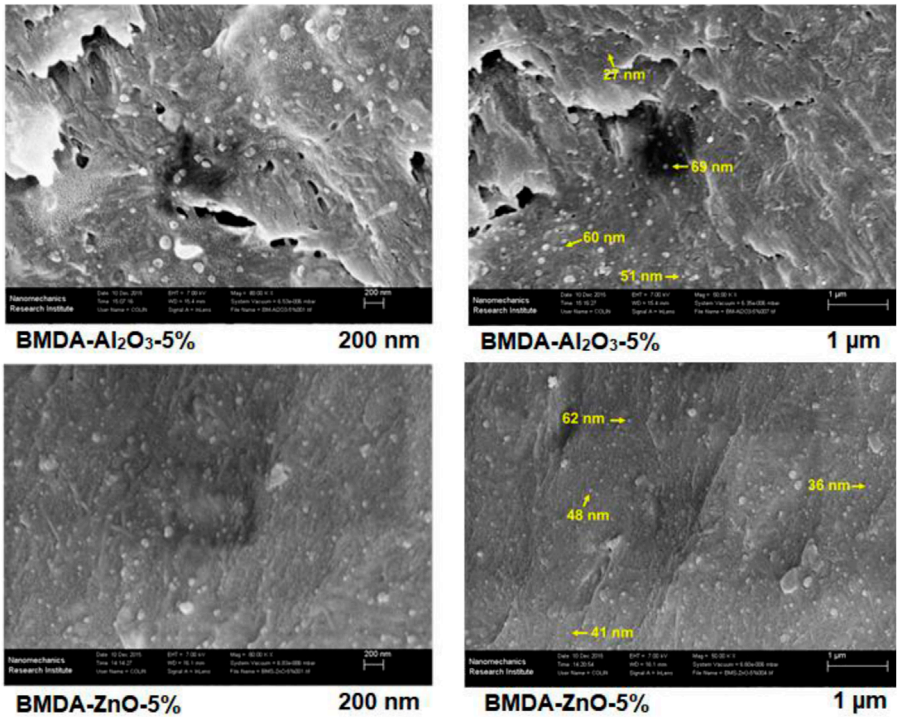

FIGURE 5
SEM images of polyimide nanocomposites at different magnification scales.

2.2 Instrumentation and measurements

Weighing and addition of BTDA were carried out under a dry and inert N_2 atmosphere inside the glove box of LabSTAR MBRAUN. Thermal curing of pre-polymer i.e., polyamic acid, was performed in the air-circulating oven of VWR, together with Lindberg furnace, which was equipped with controller (UP 150). The Fourier-transform infrared (FTIR) spectra of all the synthesized materials (polyamic acid/polyimide nanocomposites) were recorded on a Bruker Tensor 27 FTIR Spectrophotometer in the range between 400 and 4,000 cm^{-1}. The nuclear magnetic resonance (NMR) spectrum was recorded at 500 MHz in deuterated DMSO-d^6 solvent using the Bruker Avance Spectrometer. WAXRD analyses were performed using the Bruker D8 FOCUS Diffractometer, with a 2 theta (θ) range of 5°–50°, a scan speed of 3 s/step, an increment of 0.05°, and nickel-filtered Cu-*K*α radiation of 1.542 Å.

A field emission scanning electron microscope (Leo 1530 Gemini, Zeiss Germany) was used to investigate the morphology of polyimide nanocomposites. Philips CM10 Transmission Electron Microscope, which was equipped with an 11-megapixel camera, was used to determine nanoparticle dispersion within the polyimide matrix. ImageJ software was used for measuring the nanoparticle size in SEM and TEM micrographs. Thermal properties were studied by carrying out TGA on the Q500 model of the TA instrument, with a temperature increase of 20°C per minute, up to the maximum temperature of 800°C, under an N_2 atmosphere. The thermal endurance was assessed by exposing the polyimide matrix and corresponding nanocomposites at the temperature of 400°C and holding for 30 min (isothermal TGA) under an air atmosphere. The temperature was ramped up at a rate of 50°C/min. The data were measured with respect to weight loss percentage as a function of temperature for dynamic studies, while for isothermal studies, it was collected as a function of time. For differential thermogravimetric analysis (DTGA), the collected data were processed as a derivative of weight loss (%/°C). Dynamic mechanical thermal analysis (DMTA) was performed in the tensile mode over a temperature range of 35°C–400°C, at a heating rate of 5°C/min, under the air atmosphere on a rheometric dynamic mechanical thermal analyzer. The parameters of DMTA measurements were as follows: strain, 0.2%; length, 10 mm; initial static force, 0.4 N; and minimum static force, 0.01 N.

2.3 Synthesis of polyimide matrix BMDA

The protocol for the synthesis of the polyimide matrix, labeled as BMDA, as illustrated in Scheme 1, is described as follows: a 50-mL two-necked round-bottomed flask, equipped with a nitrogen tube and a magnetic stirrer, was charged with 0.198 g (1 mmol) of diamine MDA and 5 mL of solvent DMAc. After the complete dissolution of diamine, 0.322 g (1 mmol) of dianhydride BTDA was added to this solution with continuous stirring. The weighing of dianhydride and its addition to the diamine solution were performed inside the glove box to avoid the possible reaction between the dianhydride and moisture, which could lead to the formation of byproducts. The byproducts if formed could affect the properties of the final polymer. Then, the reaction mixture was stirred for another 24 h at 25°C. A transparent, viscous polyamic acid solution was obtained, which was cast onto an aluminum weighing dish and cyclodehydrated by thermal imidization to yield the final

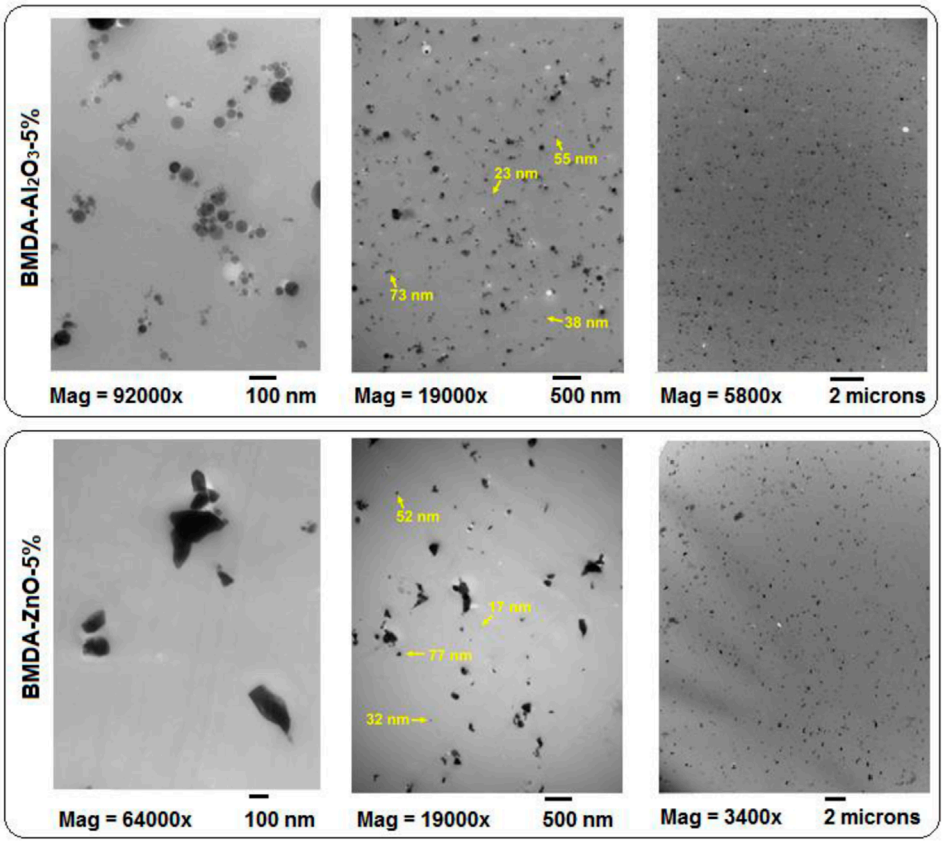

FIGURE 6
Transmission electron micrographs of nanocomposites at 100 nm, 500 nm, and 2 μm magnifications.

polyimide matrix BMDA. The thermal imidization was performed in a stepwise manner, following a programmed procedure. First, the solvent was removed by keeping the polyamic acid solution at 70°C for 18 h. Then, the polymer system was held for 1 h each at 120°C, 150°C, 200°C, 250°C, and 280°C. Finally, the aluminum sheet was carefully peeled to obtain thin solid films of polyimide with a typical amber color. Images of the polymer at different processing stages, i.e., after 70°C treatment and complete imidization, are shown in Figure 1.

2.4 Synthesis of polyimide nanocomposites

Polyimide nanocomposites (BMDA-Al_2O_3 and BMDA-ZnO) were synthesized by incorporating relevant NPs in the polyimide matrix BMDA. A schematic diagram of the synthetic protocol is illustrated in Scheme 2, and a detailed explanation of the procedure is given below.

2.4.1 General procedure

Initially, 1 mmole of MDA (0.198 g) was completely dissolved in the DMAc solvent (4 mL) taken in a round-bottom flask. To this solution, a weighed amount of Al_2O_3/ZnO nanoparticles (3%, 5%, 7%, and 9% loading) was added and sonicated for 1 h to ensure NP dispersion. Subsequently, 1 mmole of BTDA (0.322 g) was added to the as-obtained MDA-DMAc-NP suspension in small portions with continued stirring over 1 hour. The polyamic acid nanocomposite suspension was obtained by stirring the mixture at room temperature for 24 h. To achieve the nanoparticle distribution throughout the matrix, sonication was performed for another 3 h. After which, the resulting suspension of polyamic acid nanocomposite was cast onto an aluminum weighing dish, and the final polyimide nanocomposite was obtained by cyclodehydration. Curing was performed using the programmed method as follows: first, the suspension was heated at 70°C for 18 h in an air-circulating oven to remove the solvent. Then, the temperature was gradually increased to 120°C, 150°C, 200°C, 250°C, and 280°C and held for 1 h at each interval. Finally, the obtained films were peeled from the aluminum dish. Two series of polyimide nanocomposites were developed by following the aforementioned procedure. Each series comprised four members, with different concentrations of Al_2O_3/ZnO nanoparticle loading (3%, 5%, 7%, and 9%).

3 Results and discussion

3.1 FTIR spectroscopy

The structural elucidation of the synthesized polyimide matrix was carried out both at i) polyamic acid stage and ii) fully imidized form by FTIR spectroscopy. At the polyamic acid stage, the presence

TABLE 1 TGA data for dynamic studies of the pure polyimide matrix and corresponding nanocomposites showing variation in thermal stability by nanocomposite engineering.

Polymer	T_5 (°C)	T_{10} (°C)	R_{800} (%)
BMDA	540	572	62
BMDA-Al_2O_3-3%	542	574	63
BMDA-Al_2O_3-5%	542	573	64
BMDA-Al_2O_3-7%	543	574	65
BMDA-Al_2O_3-9%	548	578	67
BMDA-ZnO-3%	455	500	62
BMDA-ZnO-5%	462	512	63
BMDA-ZnO-7%	467	517	63
BMDA-ZnO-9%	462	513	66

T_5 is the temperature at 5% weight loss.
T_{10} is the temperature at 10% weight loss.
R_{800} is the residual weight (%) at 800°C.

of absorption peaks at 1,627 cm^{-1}, which are ascribed to carboxylic acid and amide moieties, verified the condensation of diamine and dianhydride, i.e., the development of the pre-polymer. The broad absorption band at 3,475 cm^{-1} is ascribed to NH and OH moieties of polyamic acid. The cyclodehydration of the pre-polymer to final polyimide was confirmed by the appearance of peaks at 1,707 cm^{-1} and 1,778 cm^{-1} in the characteristic region of the imide ring (symmetric and asymmetric stretches, respectively), along with the disappearance of amic acid bands at 1,627 cm^{-1} and 3,475 cm^{-1}. Small shoulder peaks at 1,655 cm^{-1} and 1,597 cm^{-1} in the FTIR spectrum of BMDA after imidization are attributed to the stretching vibrations of aromatic C=C conjugated with C=O and C=C of the benzene ring, respectively. The absorption band at 1,370 cm^{-1} is ascribed to the C-N-C moiety of the imide group. The FTIR spectrum of BMDA at the polyamic acid stage (BMDA-PAA) and after imidization (BMDA-PI) is shown in Figure 2.

3.2 ^{1}H NMR spectroscopy

Further evidence in favor of the polyimide structure was obtained from NMR spectroscopy. ^{1}H NMR spectra of the polyimide matrix were obtained at the polyamic acid stage because the final polymer (polyimide) was insoluble in common organic solvents. The development of the amide linkage was confirmed by the appearance of signals at 10.48 ppm and 13.34 ppm, corresponding to the protons of amide groups and carboxylic acid moieties in the polyamic acid structure, respectively (Kumar et al., 2016). Aromatic ring protons displayed signals in their characteristic region of 7.18–8.05 ppm, with respect to their locality within the polymer structure and type of neighboring groups. A singlet signal at 3.88 ppm is ascribed to protons of the -CH_2 group in the polyamic acid structure, inherited from diamine MDA. The ^{1}H NMR spectrum of the polyimide matrix BMDA at the polyamic acid stage, illustrating the assignment of specific protons, is presented in Figure 3, which approves the anticipated polymeric structure.

3.3 X-ray diffraction studies

The common and simplest technique used for investigating nanocomposite structures is WAXRD analysis. Therefore, it was used to evaluate the insertion of Al_2O_3 and ZnO nanoparticles in the polyimide matrix. The X-ray diffraction patterns of the parent matrix BMDA and relevant nanocomposites, i.e., BMDA-Al_2O_3-9% and BMDA-ZnO-9%, are presented in Figure 4. The presence of Al_2O_3 nanoparticles in the matrix was confirmed by the appearance of diffraction peaks at 2 theta values near 31.9°, 37.6°, and 45.7°, which are characteristic peaks for cubic Al_2O_3. All the peaks were indexed with the standard XRD pattern of Al_2O_3 with JCPDS No. 29–0063, as shown in Figure 4 (Hui et al., 2016). The ZnO nanoparticles manifested their presence by showing the typical signals at 2 theta values of 31.8°, 34.3°, 36.3°, and 47.5° which are characteristic peaks for the hexagonal wurtzite-type structure. All the peaks were indexed with the standard XRD pattern of zinc oxide with JCPDS No. 75–1,526, as shown in Figure 4 (Mallakpour and Hatami, 2013; Gao et al., 2010; Pal et al., 2017a; Pal et al., 2017b). The aforementioned peaks of nanoparticles were not observed in the parent polyimide matrix BMDA, thereby confirming the successful preparation of polyimide-Al_2O_3 and polyimide-ZnO nanocomposites by WAXRD.

3.4 Morphology studies by SEM and TEM

The distribution of nanoparticles within the polyimide matrix was examined through scanning electron microscopic studies. Figure 5 presents the SEM images of polyimide nanocomposites at a nanoparticle loading of 5% and different magnification scales of 200 nm and 1 µm. These graphics illustrate the dispersion of both types of nanoparticles, i.e., Al_2O_3 and ZnO, throughout the polyimide matrix. SEM micrographs for different contents of Al_2O_3 and ZnO nanoparticle samples, i.e., BMDA-Al_2O_3-9% and BMDA-ZnO-9% (Supplementary Figures S1, S2), displayed similar patterns. This further verifies the presence of nanostructured inorganic moieties throughout the polyimide matrix. Moreover, the size of the nanoparticles was measured using ImageJ software. The arrows in Figure 5 indicate some of the nanoparticles having size 27, 41, 51, and 62 nm (Ma et al., 2008).

Further evaluation regarding the dispersion of nanoparticles inside the polyimide matrix BMDA was performed through transmission electron microscopic studies. Figure 6 presents the TEM images of polyimide nanocomposites at magnification scales of 100 nm, 500 nm, and 2 µm. Like SEM, TEM also confirmed the dispersion of both types of nanoparticles, i.e., Al_2O_3 and ZnO, throughout the matrix. Few clumps of nanoparticles were observed at a 2-µm scale; however, some clusters can be observed at 500 nm, which is attributed to the agglomerate formation by more than one nanoparticle (Hsu et al., 2005; Ma et al., 2008). These agglomerates are more pronounced for ZnO nanoparticles compared to Al_2O_3 (Figure 6), which can be attributed to the high surface energy of ZnO, as suggested by Ponnamma et al. (2019),

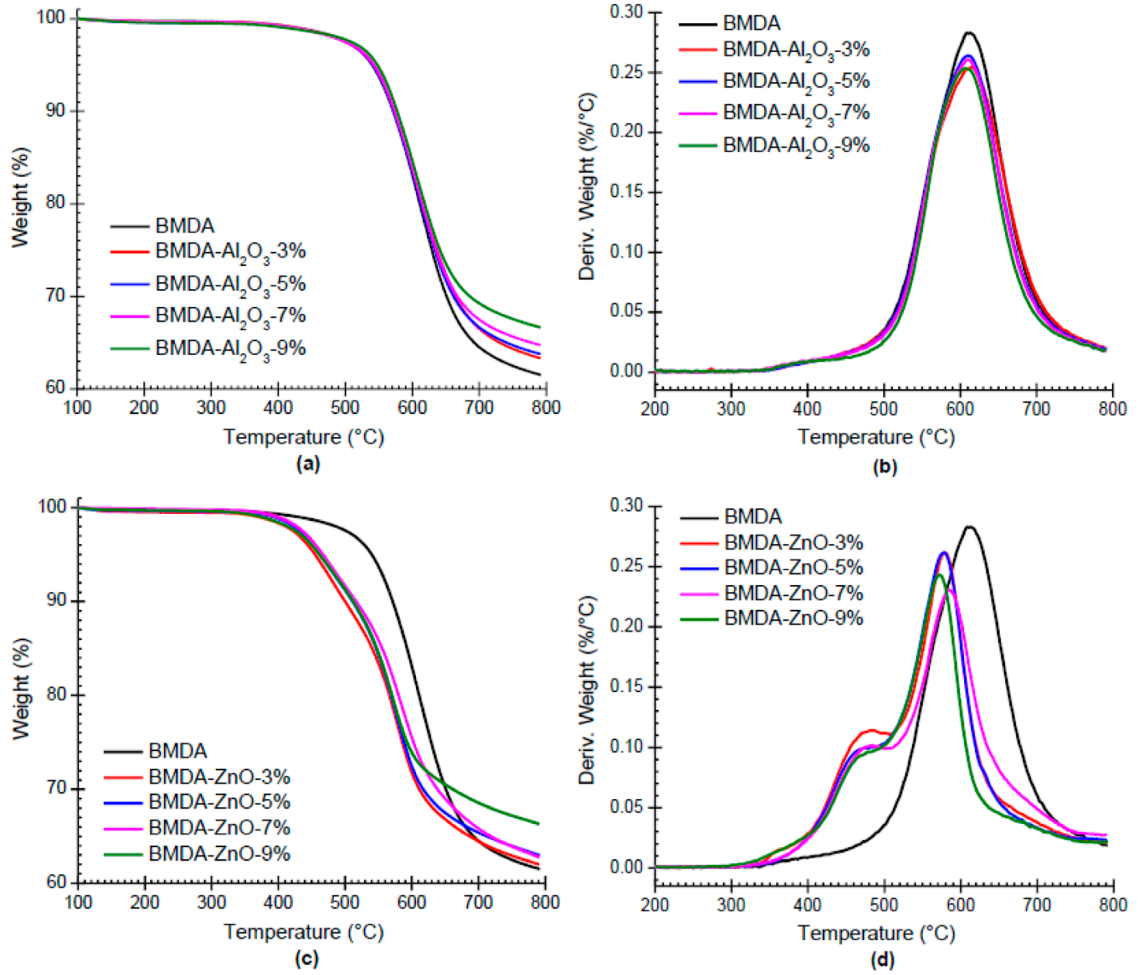

FIGURE 7
(a–d) Dynamic TGA curves **(a, c)** and DTG curves **(b, d)** illustrating variation in the thermal performance of polyimide BMDA by the addition of nanoparticles (N_2, 20°C/min).

TABLE 2 TGA data for isothermal studies demonstrating the improved thermal endurance of the polyimide matrix as a function of nanoparticle concentration.

Polymer	W_{15} (%)	W_{25} (%)	W_{35} (%)
BMDA-400	2.24	2.42	2.56
BMDA-Al_2O_3-3%-400	1.74	1.95	2.09
BMDA-Al_2O_3-5%-400	1.70	1.90	2.03
BMDA-Al_2O_3-7%-400	1.62	1.83	1.98
BMDA-Al_2O_3-9%-400	1.54	1.75	1.88

W_{15} is the weight loss (%) after 15 min of experiment.
W_{25} is the weight loss (%) after 25 min of experiment.
W_{35} is the weight loss (%) after 35 min of experiment.

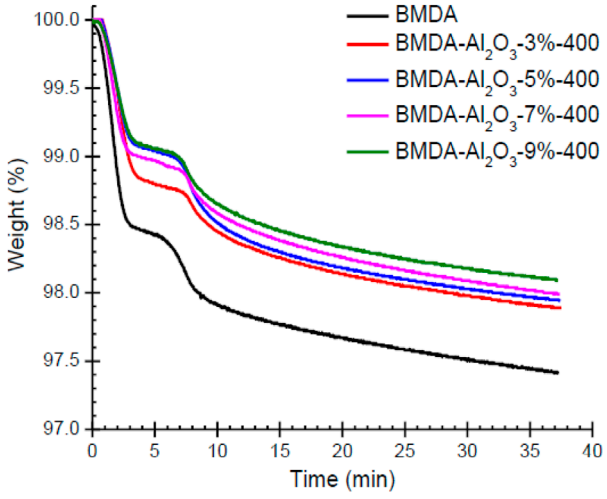

FIGURE 8
Isothermal TGA plots illustrating the improved thermal endurance of the polyimide matrix by the addition of nanoparticles (isothermal at 400°C, air, ramp at 50°C/min).

making them prone to significant agglomeration (Chen et al., 2017). The size of nanoparticles determined using ImageJ software in TEM micrographs was found to be 17, 23, 38, 52, and 77 nm (Figure 6),

TABLE 3 Mechanical damping (tan δ) data of BMDA-Al_2O_3 and BMDA-ZnO nanocomposites depicting variation in T_g with increasing concentrations of nanoparticles.

Polymer	T_g (°C)	Polymer	T_g (°C)
BMDA	293	BMDA	293
BMDA-Al_2O_3-3%	335	BMDA-ZnO-3%	341
BMDA-Al_2O_3-5%	357	BMDA-ZnO-5%	384
BMDA-Al_2O_3-7%	348	BMDA-ZnO-7%	403
BMDA-Al_2O_3-9%	331	BMDA-ZnO-9%	394

T_g is the glass transition temperature.

which is in good agreement with SEM findings. Furthermore, the 100-nm scale images of Figure 6 reveal the shapes of nanoparticles: spherical geometry was observed for Al_2O_3 nanoparticles, whereas ZnO nanoparticles displayed a flat/disk-like morphology.

Observations indicate that the use of nanoparticles without their surface modification results in the formation of larger agglomerates within polyimide matrices. However, in our case, the thorough dispersion of even unmodified nanoparticles has been illustrated by both SEM and TEM techniques. It can be inferred that the experimental procedure followed in this study developed nanocomposites with effective nanoparticle dispersion in the polyimide matrix. The probable reason is that nanoparticles can be more easily and efficiently distributed in polyamic acid with a lower molecular weight which is formed at the start of the reaction processing.

3.5 Evaluation of thermal stability

The thermal behavior of polymers was explored by two types of TGA, i.e., dynamic temperature scan and isothermal TGA. These measurements were performed to evaluate the performance of developed polyimide nanocomposites for their applications under specific conditions of high thermal stability. Most often, exposure of a few minutes does not cause much degradation of a polymeric system; however, it fails in the case of extended exposure at elevated temperatures.

3.5.1 Dynamic TGA

For the assessment of thermal stability under the N_2 atmosphere, polyimide weight change was recorded with a temperature increase from 50°C to 800°C at a heating rate of 20°C/minute. The data collected were examined as a weight loss percentage (%) for dynamic TGA, while a derivative of weight loss (%/°C) was used for DTG. The temperatures were measured at two different weight losses, i.e., 5% weight loss symbolized as T_5 and 10% weight loss abbreviated as T_{10}. From an application perspective, after the 10% weight loss, there are few chances that a resin would retain significant structural integrity.

The developed polyimide matrix displayed impressive temperature resistance as degradation started at approximately 450°C and continued with little weight loss up to 550°C. This high thermal stability is accredited to aromatic and imide moieties in polymer chains (Mathews et al., 2007; Yang and Su, 2005). The parent polyimide matrix BMDA displayed a weight loss of 5% at 540°C, whereas T_{10} was found to be at 572°C (Table 1). The char yield, i.e., the amount of residue left after decomposition, was measured to be 62% at 800°C (R_{800}).

The thermal stability of the polyimide matrix (BMDA) was further improved by the addition of Al_2O_3 nanoparticles, as illustrated by thermograms in Figures 7A, B. At a 9% loading of nanoparticles, i.e., BMDA-Al_2O_3-9%, T_5 improved from 540°C to 548°C, while T_{10} increased from 572°C to 578°C (Li et al., 2007; Wu et al., 2005). The higher heat conductivity of Al_2O_3 could possibly be responsible for this enhanced thermal stability as it rapidly transmits heat from one region to nearby areas. This prevents the backbone structure of polyimide from being damaged by heat (Hui et al., 2016). Nevertheless, the incorporation of ZnO nanoparticles into BMDA lowered its temperature resistance, as shown in the TGA and DTG plots in Figures 7C, D and the tabulated data in Table 1. The temperatures for 5% and 10% weight loss (T_5 and T_{10}) at a 9% loading level decreased from 540°C to 462°C and from 572°C to 513°C, respectively. Hsu et al. (2005) observed the same thermal pattern for nanohybrid films of BTDA-ODA/ZnO as the thermal stability of the BTDA-ODA matrix was decreased by the addition of ZnO nanoparticles. They ascribed this decrease to i) the induction of oxidation by metallic compounds, which can cause the oxidative degradation of polyimide and ii) the desorption of species present on ZnO nanoparticles. Similar behavior, i.e., decreased thermal stability of pure polyimide by ZnO nanoparticles (555°C–505°C), was reported by Somwangthanaroj et al. (2008) and was attributed to the induction of oxidative degradation and acidic hydrolysis (chain scission) of polyimide through the incorporation of metallic compounds. The pattern of TGA curves presented in Figure 7A suggests the single-step mechanism of degradation for the parent matrix BMDA and nanocomposites of Al_2O_3 (BMDA-Al_2O_3), which was further complemented by relevant DTG curves in Figure 7B. However, a two-step pathway is proposed for nanocomposites derived from ZnO, i.e., BMDA-ZnO, as illustrated in Figures 7C, D.

3.5.2 Isothermal TGA

Since Al_2O_3 nanoparticles improved the thermal stability of the polyimide matrix, only Al_2O_3 nanocomposites (BMDA-Al_2O_3) were evaluated by isothermal TGA. The obtained results are shown in Table 2 and Figure 8. The isothermal TGA curves indicated lesser weight loss for polyimide-Al_2O_3 nanocomposites compared to BMDA (parent polyimide matrix) after the same exposure at 400°C (30 min). The data presented in Table 2 indicate that a weight loss of only 1.88% was recorded after 35 min of the experiment (W_{35}) for Al_2O_3 nanocomposite with 9% loading, i.e., BMDA-Al_2O_3-9%, compared with a W_{35} value of 2.56% for BMDA (parent polyimide). These results also validate the findings of dynamic TGA, representing the higher thermal endurance of polyimide-Al_2O_3 nanocomposites than BMDA.

TGA findings have depicted that the temperature resistance (thermal stability/thermal endurance) of polyimide can be modified/tailored/tuned by nanocomposite engineering (by adjusting the type or concentration of NPs) as per the requirement of a particular application.

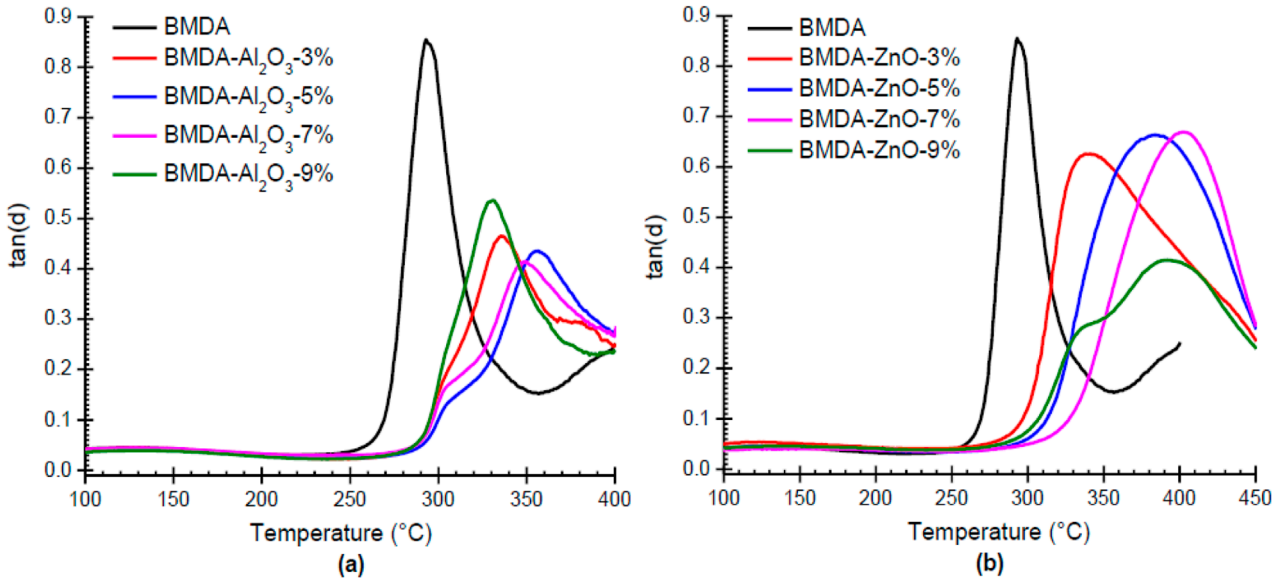

FIGURE 9
(A, B) Tan δ plots illustrating the impact of Al_2O_3 nanoparticles **(A)** and ZnO nanoparticles **(B)** on the T_g value of pure polyimide (5°C/min, air).

3.6 Dynamic mechanical thermal analysis

Thin films of the polyimide matrix and nanocomposites were prepared by the cyclodehydration of relevant polyamic acid solutions under precisely controlled conditions. DMTA was used to measure their stiffness at high temperatures, and collected data are tabulated in Table 3. Figure 9 presents the comparative mechanical damping, i.e., tan δ curves for BMDA-Al_2O_3 and BMDA-ZnO nanocomposites. The maximum temperature for the peak at the tan δ curve was noted as glass transition temperature (T_g). Embedding nanoparticles within polyimide triggered T_g enhancement, as shown by tan δ curves in Figure 9A for Al_2O_3 nanoparticles and Figure 9B for ZnO nanoparticles. The T_g values provided in Table 3 show that Al_2O_3 nanoparticles improved the T_g value of polyimide from 293°C to 357°C at 5% loading, and it was further increased to 384°C by the ZnO nanoparticles at a similar loading level (5%). This observation suggests that nanoparticles of ZnO are more effective in improving the T_g value of polyimide. This T_g enhancement is ascribed to the inter-chain interactions developed through OH groups on the nanoparticle's surface and carbonyl of imide moieties in the polymer structure (Hsu et al., 2005). Cross linking, as developed, constrained the chain flexibility/mobility of polyimide and consequently increased the T_g value of the polyimide system. T_g has increased in a concentration-dependent manner up to the optimum level of nanoparticle loading, which was found to be 5% for Al_2O_3 and 7% for ZnO. After this, the glass transition temperature started to decrease with the further addition of nanoparticles. This could be ascribed to the fact that nanoparticles remained more dispersed within the matrix up to the optimal concentration. After a specific concentration, nanoparticles possibly started interacting with each other despite the matrix, resulting in the formation of agglomerates, as shown in TEM images in Figure 6 (Ma et al., 2008; Tsai et al., 2011).

Based on these DMTA findings, it can be conveniently inferred that nanoparticles can easily regulate/modify the glass transition temperature of the polyimide matrix as per the need of a particular application. The objective can be achieved either by selecting a specific nanoparticle or varying the concentration of any selected nanoparticle.

4 Conclusion

Nanocomposite engineering effectively tailored the properties of the polyimide film. The successful synthesis of parent polyimide and relevant nanocomposites was established by structural elucidations using FTIR and NMR spectroscopic techniques. WAXRD, SEM, and TEM studies verified the incorporation of Al_2O_3 and ZnO nanoparticles, along with their distribution throughout the polyimide matrix. The developed polyimide matrix displayed impressive thermal stability as the degradation started at approximately 450°C and continued with small weight loss up to 550°C. The thermal stability and thermal endurance of the pure polyimide matrix were further enhanced by incorporating Al_2O_3 nanoparticles. However, the addition of ZnO nanoparticles lowered the temperature resistance of the same matrix. The findings of dynamic TGA studies were validated by isothermal TGA, representing the greater thermal stability of polyimide-Al_2O_3 nanocomposites than parent polyimide. The glass transition temperature of the polyimide matrix was enhanced by both types of nanoparticles in a concentration-dependent manner, with ZnO being more effective than Al_2O_3.

Overall, the presented research aligns with the manuscript's scope, demonstrating that polyimide properties can be customized/tailored/tuned to desired ones through nanocomposite

engineering. The synthesized polyimide nanocomposite films show tremendous potential as high-temperature-resistant materials for applications in extreme conditions, where exceptional thermal stability is required for extended periods. However, their widespread adoption may be limited due to high production costs, challenges with nanoparticle dispersion, scalability issues, and environmental concerns. Future research should focus on overcoming these challenges to enable broader applications. In addition, exploring the UV-shielding and flame-retardant properties of the synthesized materials could further expand their range of applications in automotive and aerospace industries.

Data availability statement

The original contributions presented in the study are included in the article/supplementary material; further inquiries can be directed to the corresponding authors.

Author contributions

AA: writing–original draft, writing–review and editing, conceptualization, data curation, formal analysis, investigation, methodology, project administration, resources, software, validation, and visualization. ZA: conceptualization, investigation, methodology, project administration, resources, visualization, writing–original draft, writing–review and editing, and supervision. MF: data curation, validation, visualization, and writing–review and editing. LS: conceptualization, data curation, investigation, methodology, project administration, resources, supervision, and writing–review and editing. KM: visualization, writing–review and editing, formal analysis, and validation. MN: formal analysis, visualization, writing–review and editing, funding acquisition, and writing–original draft.

Funding

The author(s) declare that financial support was received for the research and/or publication of this article. AA is thankful for financial support provided under International Research Support Initiative Program (IRSIP) and Indigenous 5000 Ph.D. Fellowship Program (Phase II) by Higher Education Commission of Pakistan.

Conflict of interest

The authors declare that the research was conducted in the absence of any commercial or financial relationships that could be construed as a potential conflict of interest.

Generative AI statement

The author(s) declare that no Generative AI was used in the creation of this manuscript.

Publisher's note

Supplementary material

The Supplementary Material for this article can be found online at: https://www.frontiersin.org/articles/10.3389/fmats.2025.1504965/full#supplementary-material

References

Aframehr, W. M., Molki, B., Bagheri, R., Heidarian, P., and Davodi, S. M. (2020). Characterization and enhancement of the gas separation properties of mixed matrix membranes: polyimide with nickel oxide nanoparticles. *Chem. Eng. Res. Des.* 153, 789–805. doi:10.1016/j.cherd.2019.11.006

Ashraf, A. R., Akhter, Z., Mckee, V., and Siddiq, M. (2015). Effect of polydimethylsiloxane incorporation on the properties of polyimides synthesized from newly designed α,α′-bis(2-aminophenoxy)-p-xylene. *Express Polym. Lett.* 9, 1001–1014. doi:10.3144/expresspolymlett.2015.90

Ashraf, A. R., Akhter, Z., Simon, L. C., Castel, C. D., and Assoud, A. (2018b). Polyimide derivatives of 4,4′-bis((4-aminophenoxy)methyl)-1,1′-biphenyl: synthesis, spectroscopic characterization, single crystal XRD and thermal studies. *J. Mol. Struct.* 1169, 46–58. doi:10.1016/j.molstruc.2018.05.051

Ashraf, A. R., Akhter, Z., Simon, L. C., McKee, V., and Castel, C. D. (2018a). Synthesis of polyimides from α,α′-bis(3-aminophenoxy)-p-Xylene: spectroscopic, single crystal XRD and thermal studies. *J. Mol. Struct.* 1160, 177–188. doi:10.1016/j.molstruc.2018.01.098

Chang, Z., Sun, X., Liao, Z., Liu, Q., and Han, J. (2022). Design and preparation of polyimide/TiO2@MoS2 nanofibers by hydrothermal synthesis and their photocatalytic performance. *Polym. (Basel)* 14, 3230. doi:10.3390/polym14163230

Chen, M., Zhou, W., Zhang, J., and Chen, Q. (2020). Dielectric property and space charge behavior of polyimide/silicon nitride nanocomposite films. *Polym. (Basel)* 12, 322. doi:10.3390/polym12020322

Chen, X., Zhu, W., Chen, J., Cao, Q., Chen, Y., and Hu, D. (2022). TiO2 nanoparticle/polyimide nanocomposite for ultrahigh-temperature energy storage. *Nanomaterials* 12, 4458. doi:10.3390/nano12244458

Chen, Y., Ding, H., and Sun, S. (2017). Preparation and characterization of ZnO nanoparticles supported on amorphous SiO2. *Nanomaterials* 7, 217. doi:10.3390/nano7080217

Elbakoush, F. E., Khan, Q. U., Ullah, M., Ullah, A., Khan, A. U., Khan, J., et al. (2021). Characterization and thermal degradation study of carbonization the polyimide (PMDA/ODA)/Fe composite films. *Trans. Electr. Electron. Mater.* 22, 843–850. doi:10.1007/s42341-021-00309-0

Faghihi, K., and Hajibeygi, M. (2013). Synthesis and properties of polyimide/silver nanocomposite containing dibenzalacetone moiety in the main chain. *J. Saudi Chem. Soc.* 17, 419–423. doi:10.1016/j.jscs.2011.05.005

Gao, C., Zhu, J., Ye, S., Li, M., Wang, H., and He, J. (2025). Novel high-entropy perovskite titanate: a potential thermal protective material with improved thermophysical properties. *J. Eur. Ceram. Soc.* 45, 116878. doi:10.1016/j.jeurceramsoc.2024.116878

Gao, H., Yorifuji, D., Wakita, J., Jiang, Z. H., and Ando, S. (2010). *In situ* preparation of nano ZnO/hyperbranched polyimide hybrid film and their optical properties. *Polym. Guildf.* 51, 3173–3180. doi:10.1016/j.polymer.2010.05.019

Hager, C. J., McMillen, C. D., Sachdeva, R., Martin, A. W., and Thrasher, J. S. (2023). New fluorine-containing diamine monomers for potentially improved polyimides. *Molecules* 28, 6855. doi:10.3390/molecules28196855

Hsu, S. C., Whang, W. T., Hung, C. H., Chiang, P. C., and Hsiao, Y. N. (2005). Effect of the polyimide structure and ZnO concentration on the morphology and characteristics of polyimide/ZnO nanohybrid films. *Macromol. Chem. Phys.* 206, 291–298. doi:10.1002/macp.200400326

Hui, S., Lizhu, L., Ling, W., Weiwei, C., and Xingsong, Z. (2016). Preparation and characterization of polyimide/Al2O3 nanocomposite film with good corona resistance. *Polym. Compos.* 37, 763–770. doi:10.1002/pc.23233

Huo, G., Xu, S., Wu, L., Kang, S., Zhang, Z., Fan, Y., et al. (2022). Structural engineering on copolyimide membranes for improved gas separation performance. *J. Memb. Sci.* 643, 119989. doi:10.1016/J.MEMSCI.2021.119989

Jeon, H., Yoon, C., Song, Y. G., Han, J., Kwon, S., Kim, S., et al. (2018). Reducing the coefficient of thermal expansion of polyimide films in microelectronics processing using ZnS particles at low concentrations. *ACS Appl. Nano Mater.* 1, 1076–1082. doi:10.1021/acsanm.7b00259

Jeon, I., and Baek, J. (2010). Nanocomposites derived from polymers and inorganic nanoparticles. *Mater. (Basel)* 3, 3654–3674. doi:10.3390/ma3063654

Kango, S., Kalia, S., Celli, A., Njuguna, J., Habibi, Y., and Kumar, R. (2013). Surface modification of inorganic nanoparticles for development of organic – inorganic nanocomposites — a review. *Prog. Polym. Sci.* 38, 1232–1261. doi:10.1016/j.progpolymsci.2013.02.003

Kickelbick, G. (2003). Concepts for the incorporation of inorganic building blocks into organic polymers on a nanoscale. *Prog. Polym. Sci.* 28, 83–114. doi:10.1016/s0079-6700(02)00019-9

Kim, S. D., Kim, S. Y., and Chung, I. S. (2013). Soluble and transparent polyimides from unsymmetrical diamine containing two trifluoromethyl groups. *J. Polym. Sci. Part A Polym. Chem.* 51, 4413–4422. doi:10.1002/pola.26855

Kim, Y. J., Kim, J. H., Ha, S. W., Kwon, D., and Lee, J. K. (2014). Polyimide nanocomposites with functionalized SiO2 nanoparticles: enhanced processability, thermal and mechanical properties. *RSC Adv.* 4, 43371–43377. doi:10.1039/c4ra04952g

Kumar, A., Tateyama, S., Yasaki, K., Ali, M. A., Takaya, N., Singh, R., et al. (2016). 1H NMR and FT-IR dataset based structural investigation of poly(amic acid)s and polyimides from 4,4′-diaminostilbene. *Data Br.* 7, 123–128. doi:10.1016/j.dib.2016.02.006

Lal, R., Rathore, B. S., and Gaur, M. S. (2012). Structural and polarization properties of polyimide/TiO2 nanocomposites. *Ionics (Kiel).* 18, 565–572. doi:10.1007/s11581-011-0649-9

Li, H. Y., Ning, S. F., Hu, H. B., Liu, B., Chen, W., and Chen, S. T. (2007). Synthesis and electrical properties of polyimide-Al2O3 composites. *Chin. J. Polym. Sci.* 25, 271–276. doi:10.1142/s0256767907002102

Li, Z., Qin, H., Song, J., Liu, M., Zhang, X., Wang, S., et al. (2022). Polyimide nanodielectrics doped with ultralow content of MgO nanoparticles for high-temperature energy storage. *Polym. (Basel)* 14, 2918. doi:10.3390/polym14142918

Lu, H. T., Huang, S. L., Tseng, I. H., Lin, Y. K., and Tsai, M. H. (2013). Properties of polyimide hybrids with mixed metal oxide. *J. Appl. Polym. Sci.* 127, 145–153. doi:10.1002/app.37865

Ma, J., Liu, X., Wang, R., Lu, C., Wen, X., and Tu, G. (2023). Research progress and application of polyimide-based nanocomposites. *Nanomaterials* 13, 656. doi:10.3390/nano13040656

Ma, P., Nie, W., Yang, Z., Zhang, P., Li, G., Lei, Q., et al. (2008). Preparation and characterization of polyimide/Al2O3 hybrid films by sol–gel process. *J. Appl. Polym. Sci.* 108, 705–712. doi:10.1002/app.27540

Mallakpour, S., and Hatami, M. (2013). Study on constructional design and structural analysis of poly (amide-imide)/ZnO nanocomposites containing pyromellitoyl-bis-l-isoleucine moieties. *High. Perform. Polym.* 25, 436–444. doi:10.1177/0954008312469235

Mallakpour, S., Madani, M., and Roshandel, S. (2014). Applications of ultrasound for modification of zinc oxide and fabrication of optically active poly(amide-imide)/zinc oxide bionanocomposites. *Des. Monomers Polym.* 17, 364–371. doi:10.1080/15685551.2013.840511

Mathews, A. S., Kim, I., and Ha, C. S. (2007). Synthesis, characterization, and properties of fully aliphatic polyimides and their derivatives for microelectronics and optoelectronics applications. *Macromol. Res.* 15, 114–128. doi:10.1007/bf03218762

Mathur, A., Pal, D., Singh, A., Sengupta, A., Singh, R., and Chattopadhyay, S. (2019). Violet emission of ALD-grown ZnO nanostructures on confined polymer films: defect origins and emission control via interface engineering based on confinement of the bottom polymer template. *Macromol. Chem. Phys.* 220, 1800435. doi:10.1002/macp.201800435

Mehmood, Z., Shah, S. A. A., Omer, S., Idrees, R., and Saeed, S. (2024). Scalable synthesis of high-quality, reduced graphene oxide with a large C/O ratio and its dispersion in a chemically modified polyimide matrix for electromagnetic interference shielding applications. *RSC Adv.* 14, 7641–7654. doi:10.1039/d4ra00329b

Morgan, A. B., and Putthanarat, S. (2011). Use of inorganic materials to enhance thermal stability and flammability behavior of a polyimide. *Polym. Degrad. Stab.* 96, 23–32. doi:10.1016/j.polymdegradstab.2010.11.005

Nikolaeva, A. L., Bugrov, A. N., Sokolova, M. P., Ivan'kova, E. M., Abalov, I. V., Vlasova, E. N., et al. (2022). Metal oxide nanoparticles: an effective tool to modify the functional properties of thermally stable polyimide films. *Polym. (Basel)* 14, 2580. doi:10.3390/polym14132580

Nikolaeva, A. L., Bugrov, A. N., Sokolova, M. P., Kuntsman, I. V., Vlasova, E. N., Ivan'kova, E. M., et al. (2023). Synergistic effect of metal oxide and carbon nanoparticles on the thermal and mechanical properties of polyimide composite films. *Polym. (Basel)* 15, 2298. doi:10.3390/polym15102298

Nikolaeva, A. L., Gofman, I. V., Yakimansky, A. V., Ivan'kova, E. M., Abalov, I. V., Baranchikov, A. E., et al. (2020). Polyimide-based nanocomposites with binary CeO2/nanocarbon fillers: conjointly enhanced thermal and mechanical properties. *Polym. (Basel)* 12, 1952. doi:10.3390/polym12091952

Ouyang, Y., Bai, L., Tian, H., Li, X., and Yuan, F. (2022). Recent progress of thermal conductive ploymer composites: Al2O3 fillers, properties and applications. *Compos. Part A Appl. Sci. Manuf.* 152, 106685. doi:10.1016/j.compositesa.2021.106685

Pal, D., Mathur, A., Singh, A., Singhal, J., Sengupta, A., Dutta, S., et al. (2017a). Tunable optical properties in atomic layer deposition grown ZnO thin films. *J. Vac. Sci. Technol. A Vac. Surfaces, Film.* 35, 01B108. doi:10.1116/1.4967296

Pal, D., Singhal, J., Mathur, A., Singh, A., Dutta, S., Zollner, S., et al. (2017b). Effect of substrates and thickness on optical properties in atomic layer deposition grown ZnO thin films. *Appl. Surf. Sci.* 421, 341–348. doi:10.1016/j.apsusc.2016.10.130

Pavlenko, V. I., Cherkashina, N. I., and Yastrebinsky, R. N. (2019). Synthesis and radiation shielding properties of polyimide/Bi2O3 composites. *Heliyon* 5, e01703. doi:10.1016/j.heliyon.2019.e01703

Phatak, K. A., Khanna, P. K., and Nath, B. B. (2024). ZnO nanoparticles: a key ingredient of sunscreen shows absence of adverse effects on Drosophila melanization pathway. *Nano-Structures and Nano-Objects* 38, 101145. doi:10.1016/j.nanoso.2024.101145

Ponnamma, D., Cabibihan, J. J., Rajan, M., Pethaiah, S. S., Deshmukh, K., Gogoi, J. P., et al. (2019). Synthesis, optimization and applications of ZnO/polymer nanocomposites. *Mater. Sci. Eng. C* 98, 1210–1240. doi:10.1016/j.msec.2019.01.081

Rafiee, Z., and Golriz, L. (2015). Polyimide nanocomposite films containing α-Fe2O3 nanoparticles. *J. Polym. Res.* 22, 630. doi:10.1007/s10965-014-0630-1

Rafiq, S., Man, Z., Maulud, A., Muhammad, N., and Maitra, S. (2012). Separation of CO2 from CH4 using polysulfone/polyimide silica nanocomposite membranes. *Sep. Purif. Technol.* 90, 162–172. doi:10.1016/j.seppur.2012.02.031

Singh, A., Mathur, A., Pal, D., Sengupta, A., Singh, R., and Chattopadhyay, S. (2019). Near room temperature atomic layer deposition of ZnO thin films on poly(methyl methacrylate) (pmma) templates: a study of structure, morphology and photoluminescence of ZnO as an effect of template confinement. *Vacuum* 161, 398–403. doi:10.1016/j.vacuum.2019.01.006

Singh, A., Schipmann, S., Mathur, A., Pal, D., Sengupta, A., Klemradt, U., et al. (2017). Structure and morphology of magnetron sputter deposited ultrathin ZnO films on confined polymeric template. *Appl. Surf. Sci.* 414, 114–123. doi:10.1016/j.apsusc.2017.04.078

Somwangthanaroj, A., Phanthawonge, C., Ando, S., and Tanthapanichakoon, W. (2008). Effect of the origin of ZnO nanoparticles dispersed in polyimide films on their photoluminescence and thermal stability. *J. Appl. Polym. Sci.* 110, 1921–1928. doi:10.1002/app.28299

Tsai, M. H., Wang, H. Y., Lu, H. T., Tseng, I. H., Lu, H. H., Huang, S. L., et al. (2011). Properties of polyimide/Al2O3 and Si3N4 deposited thin films. *Thin Solid Films* 519, 4969–4973. doi:10.1016/j.tsf.2011.01.063

Wang, H., Cao, P., Zhu, S., Ma, C., Chen, Y., and Guo, Y. (2024). Preparation of bamboo charcoal-reinforced polyamide 6 composites modified with diverse additives: synergy and interface improvement. *Ind. Crops Prod.* 222, 119851. doi:10.1016/j.indcrop.2024.119851

Wang, S., Chen, M., and Cao, K. (2022). Polymer composite with enhanced thermal conductivity and insulation properties through aligned Al2O3 fiber. *Polym. (Basel)* 14, 2374. doi:10.3390/polym14122374

Wu, J., Yang, S., Gao, S., Hu, A., Liu, J., and Fan, L. (2005). Preparation, morphology and properties of nano-sized Al2O3/polyimide hybrid films. *Eur. Polym. J.* 41, 73–81. doi:10.1016/j.eurpolymj.2004.08.014

Wu, J., Zhang, B., Li, T., Du, Y., Cao, W., and Yang, H. (2022). Effect of trap regulation on vacuum DC surface flashover characteristics of nano-ZnO/PI film. *Polym. (Basel)* 14, 3605. doi:10.3390/polym14173605

Yang, C. P., and Su, Y. Y. (2005). Colorless polyimides from 2,3,3′,4′-biphenyltetracarboxylic dianhydride (α-BPDA) and various aromatic bis(ether amine)s bearing pendent trifluoromethyl groups. *Polym. Guildf.* 46, 5797–5807. doi:10.1016/j.polymer.2005.04.076

Yousefi, F., Mousavi, S. B., Heris, S. Z., and Naghash-Hamed, S. (2023). UV-shielding properties of a cost-effective hybrid PMMA-based thin film coatings using TiO2 and ZnO nanoparticles: a comprehensive evaluation. *Sci. Rep.* 13, 7116. doi:10.1038/s41598-023-34120-z

Yuan, P., Xue, R., Wang, Y., Su, Y., Zhao, B., Wu, C. L., et al. (2024). Horizontally-oriented barium Titanate@Polydomine/polyimide nanocomposite films for high-temperature energy storage. *J. Colloid Interface Sci.* 662, 1052–1062. doi:10.1016/j.jcis.2024.02.109

Zhang, Y., Hu, T., Hu, R., Jiang, S., Zhang, C., and Hou, H. (2022). Thermal, mechanical and dielectric properties of polyimide composite films by in-situ reduction of fluorinated graphene. *Molecules* 27, 8896. doi:10.3390/molecules27248896

Zhu, S., Wu, S., Fu, Y., and Guo, S. (2024). Prediction of particle-reinforced composite material properties based on an improved Halpin–Tsai model. *AIP Adv.* 14, 45339. doi:10.1063/5.0206774